



Identification of small molecules against the NMDAR: an insight from virtual screening, density functional theory, free energy landscape and molecular dynamics simulation-based findings

Garima Sharma¹ · Rohit Shukla^{1,2} · Tiratha Raj Singh^{1,2,3}

Received: 16 November 2021 / Revised: 23 July 2022 / Accepted: 3 August 2022 / Published online: 23 August 2022
© The Author(s), under exclusive licence to Springer-Verlag GmbH Austria, part of Springer Nature 2022

Abstract

Alzheimer's disease (AD) is a chronic intensifying neurodegenerative disorder and accounts for three fourths of dementia cases. To date, there is no effective treatment available which can completely cure AD. The available medications can slow AD progression and can provide symptomatic relaxation. The N-methyl-D-aspartate receptor (NMDAR) plays a paramount role in the survival of neurons and synaptic plasticity. It is also involved in several other diseases. Although, excessive function of NMDAR cause excitotoxicity. Due to this the cell death process activated resulting into neurodegeneration and promotes AD. Hence in this study, we have screened 98,072 natural compounds using Smina and idock. After that top scoring 154 compounds were selected and ADMET analysis was carried out. It reveals that 18 compounds are good fit in all the ADMET parameters and employed for the re-docking studies using Autodock Vina. Then from the docking result, we have selected top three complexes (NMDAR-ZINC4258884, NMDAR-ZINC8635472, and NMDAR-ZINC15675934) and employed them for the 100 ns MDS studies. Based on MDS and Gibbs free energy landscape result analysis we have concluded that NMDAR-ZINC4258884 and NMDAR-ZINC15675934 are the best stable complex and can function as a lead compound against the NMDAR. Although this is a theoretical study while we have shortlisted only two compounds out of 98,072 compounds using rigorous computational approach and proposed them to the scientific community worldwide for further experimental validations.

Keywords Alzheimer's disease · Neurofibrillary tangles · Virtual screening · Molecular docking · Molecular dynamics simulation · Principal component analysis

1 Introduction

Alzheimer's disease (AD) has been outlined as a chronic intensifying neurodegenerative disease. Its onset is slow, but it worsens gradually over time (Verma et al. 2018). It has been believed to be a cause of 60–70% of dementia. The foremost common early symptom is claimed to be, “difficulty in remembering recent events”. With the advancement in illness, symptoms include Aphasia, self-negligence, and performance problems. In line with a report, in the last 10 years, casualties from cardiovascular diseases have shown a 7 to 8% decrease whereas casualties from AD are hyperbolic 145%. As per an estimate, 6.2 million Americans aged 65+ are diagnosed with AD in the year 2020. In an estimate, it is predicted that in 30 years from now, dementia (showing 60–70% contribution for AD) will be affecting approximately 152 million people worldwide. An estimated four million Indians are affected by one or another

Garima Sharma and Rohit Shukla contributed equally to the work.

✉ Tiratha Raj Singh
tiratharaj@gmail.com; tiratharaj.singh@juit.ac.in

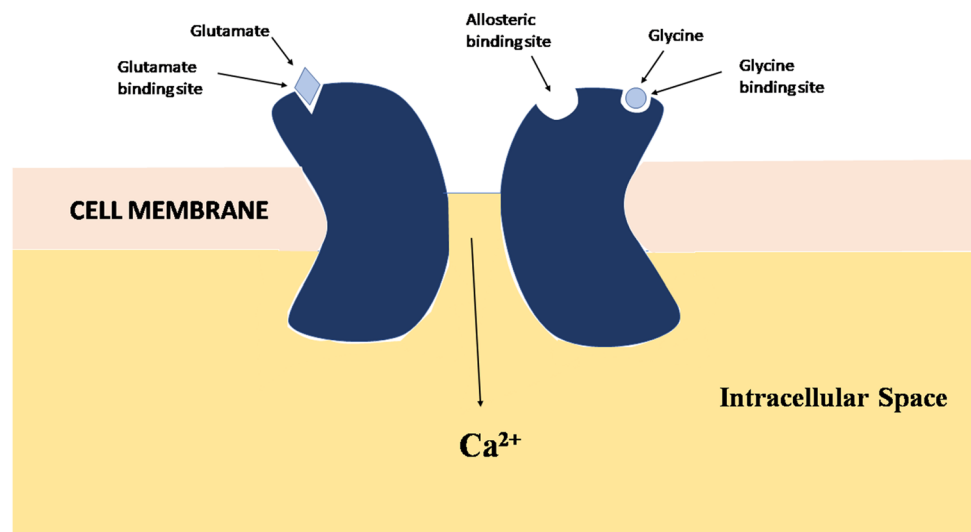
- ¹ Department of Biotechnology and Bioinformatics, Jaypee University of Information Technology (JUIT), Wagnaghat, Solan, H.P. 173234, India
- ² Centre for Excellence in Healthcare Technologies and Informatics (CEHTI), Jaypee University of Information Technology (JUIT), Wagnaghat, Solan, H.P. 173234, India
- ³ Department of Biotechnology and Bioinformatics and Centre for Excellence in Healthcare Technologies and Informatics (CEHTI), Jaypee University of Information Technology, Wagnaghat, Solan, H.P. 173215, India

form of dementia. The AD is mainly characterized by the β -amyloid plaques and neurofibrillary tangles (NFTs). One major cause of AD is an accumulation of β -amyloid protein which is (in normal condition) the metabolic waste product present in the fluid between brain cells (Cao et al. 2018). The NFTs are made by the tau protein hyperphosphorylation via the Glycogen Synthase Kinase 3 β (GSK3 β) and Cyclin dependent kinase 5 (CDK5) enzymes. The NFTs are present inside the neuronal cell and promotes the cell death. We have proposed various compounds to reduce the tau phosphorylation induced by GSK3 β (Shukla et al. 2019; Shukla and Singh 2021) and CDK5 (Shukla and Singh 2020a, b) recently. In AD, β -amyloid comes to create amyloid plaques which are thought to instigate neuroinflammation and disrupt the information exchange among neurons (Weller and Budson 2018). Now, in the neuron, NMDAR which is a type of ionotropic glutamate receptor (iGluR) whose function involves the mediation of the excitatory transmission in the brain is present (Wang and Reddy 2017). The protagonist molecule NMDA (N-methyl-D-aspartate) binds selectively to the NMDA receptors only; hence it is named as NMDA receptor. NMDA receptors are activated upon the binding of the glutamate and glycine (or D serine) with these receptors; upon activation they allow the flow of the positively charged ions through them. They have an important role in forming memory, learning, and synaptic plasticity (Fig. 1) (Newcomer et al. 2000).

NMDAR is thought to be different from other ionotropic glutamate receptors as it has voltage-dependent activation through Mg^{2+} blockade removal, high Ca^{2+} permeability and comparably slow ligand-gated kinetics. In normal condition, the resting membrane potential is -70 mV, at this potential the NMDAR Ca^{2+} channel is thought to be blocked by Mg^{2+} (Blanke and VanDongen 2009). In the Long-Term Potential (LTP), there is a strong and long-lasting release of glutamate

from the presynaptic terminal, which activates α -amino-3-hydroxy-5-methyl-4-isoxazolepropionic acid receptor (AMPA) and subsequent withdrawals of glutamate, which ultimately removes the Mg^{2+} inhibition of NMDAR and thus allows the entry of Ca^{2+} , which ultimately leads to improved synaptic strength (Abbott et al. 2008). Studies suggest that β -amyloid proteins which accumulate in the brains of AD patients can cause abnormal increase in synaptic glutamate levels by blocking glutamate uptake or making glutamate free from glial cells (Danysz and Parsons 2012). The binding of glutamate to the NMDA receptor triggers the extracellular Ca^{2+} flight that regulates membrane permeability and synaptic transmission (Danysz and Parsons 2012). When glutamate levels increase abnormally, in addition to reactivation of NMDA receptors leading to an overgrowth of Ca^{2+} substances that remove Mg^{2+} inhibition, ultimately leading to cell division and death (Zhang et al. 2016). More influx of Ca^{2+} occurs since NMDARs increased the penetration of Ca^{2+} compared to other iGluR (Liu et al. 2019). Therefore, blocking this receptors can be a potential treatment for AD, thus stopping the excessive influx of Ca^{2+} (Folch et al. 2016; Kumar et al. 2016; Jewett and Thapa 2021). Previously various clinical trials for the inhibitor identification have been carried out for the involvement of NMDAR in various disease while no success have been achieved (Ikonomidou and Turski 2002). The memantine is an FDA approved antagonist which blocks the NMDAR activity and gives the symptomatic relax in the case of AD. Although it has several side effects. There are several compounds have been identified in the previous years and are in clinical trial against the NMDAR. The NitroMemantine has been proposed against the NMDAR in the case of cardiovascular disease (Takahashi et al. 2015). It showed prominent results to block the NMDAR function. The combination of dextromethorphan (DMP) and bupropion called AXS-05 is a well-known

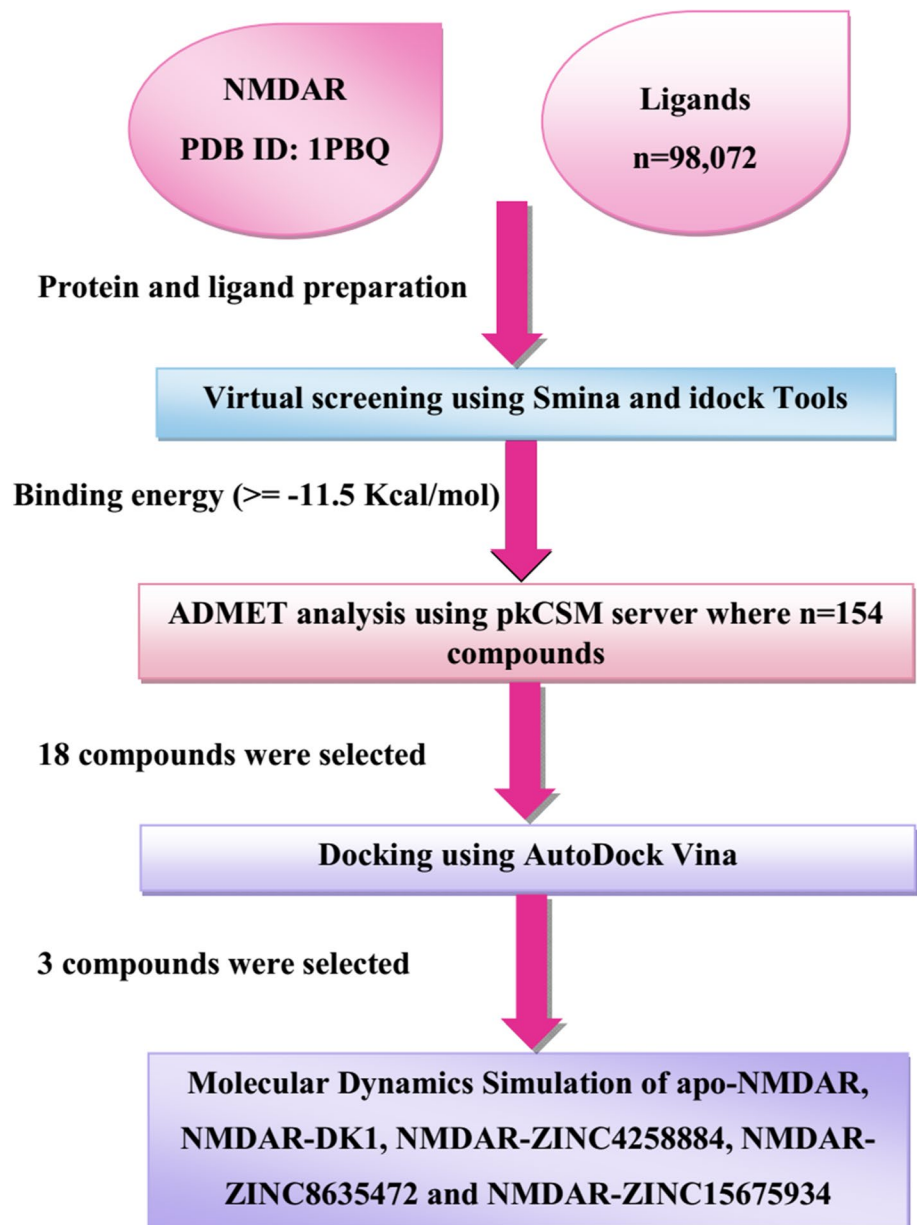
Fig. 1 An illustrative diagram to represent the NMDAR activation and its binding site



antagonist of NMDAR (Tabuteau et al. 2022). The Ketamine (Kato and Duman 2020), Dextromethorphan or Magnesium are famous antagonist for the NMDAR. Effect of oral magnesium for blocking the NMDAR has been assessed by a clinical trial study related to breast cancer (Morel et al. 2018). The RL-208 is found potent as the NMDAR antagonist in the SAMP8 mice (Companys-Aleman et al. 2020). Additionally, several studies have been going on to find the new NMDAR inhibitors therefore in our study also we are proposing new compounds through a rigorous computational analysis.

We have used the structure-based virtual screening approach and 98,072 compounds were screened against the NMDAR. After those 154 compounds were chosen for the ADMET (Absorption, Distribution, Metabolism, Excretion, and Toxicity) analysis and then selected 18 compounds were used for the re-docking studies using the AutoDock Vina. Finally, 3 compounds were selected and used for the 100 ns simulation. Lastly, based on MDS results we have proposed that NMDAR-ZINC4258884 and NMDAR-ZINC15675934 complexes are showing stability and these compounds can function as novel as well as potential compounds against the NMDAR. A comprehensive methodology is shown in Fig. 2.

Fig. 2 A complete workflow of the methodology



2 Methodology

2.1 Preparation and retrieval of ligand and protein

The RCSB protein data bank (PDB) was used to download the structure of the NMDA receptor protein (PDB ID:1PBQ, 1.90 Å, X-ray) (Armstrong and Gouaux 2000). The DK1 (5,7-Dichloro-4-Hydroxyquinoline-2-Carboxylic Acid) is an experimentally proved inhibitor and co-crystallized with this structure. The preparation of structure is done using Chimera 1.13.1 software (Pettersen et al. 2004). Then, using Amber ff99SB force field (Lindorff-Larsen et al. 2010) the structure was subjected to minimization using Chimera 1.13.1. After the minimization step, further protein structure is used in AutoDock Tools to convert from PDB to *.pdbqt*. The ZINC database (Sterling and Irwin 2015) is used to download the structure of 98,072 compounds in *.mol2* format. These ligands were converted from *mol2* to *.pdbqt* file format for the screening using a Python script (<http://autodock.scripps.edu/faqs-help/how-to/how-to-prepare-a-ligand-file-for-autodock4>).

2.2 Analysis of binding site for 1PBQ

The NMDA receptor protein is co-crystallized with its known inhibitor DK1. Therefore, the binding cavity related to DK1 is selected for virtual screening. We check for the DK1 associated cavity by analyzing the DK1 interactions with NMDAR. For the grid preparation of 1PBQ, numerous residues like Gln13, Asp224, Phe92, and Ser180, etc. were selected.

2.3 Virtual screening

Virtual screening is an efficient process to find a potent inhibitor using computational approaches (Shukla et al. 2018, 2021). It is an efficient and less time-consuming process where we can screen a large compound dataset within few days. Here we have used Smina - A fork of AutoDock Vina and idock (Li et al. 2012) for the virtual screening. They both are inspired from the Autodock Vina (Trott and Olson 2010) method but they are less time-consuming than Autodock Vina. The idock is a multithreaded and improved algorithm for virtual screening and very fast compared to all other available tools. It can screen a compound within seconds. The user can define the computer threads and based on a defined core it can screen thousands of compounds within hours. Hence, we have used these softwares for the virtual screening and then 154 compounds which

were showing the ≥ -11.5 kcal/mol binding affinity were adopted selected for the ADMET analysis.

2.4 ADMET prediction

The ADMET prediction was done of the 154 ZINC compounds using the pkCSM tool (<http://biosig.unimelb.edu.au/pkcsm/prediction>), which is an ADMET predicting web-based server (Pires et al. 2015). This software is freely available and to perform the prediction user can provide the ligand with the SMILES string or draw the chemical structure on the screen. This web server contains a large dataset of compounds approved by the FDA. Also, the dataset is available from scientific literature present in PubMed (<https://pubmed.ncbi.nlm.nih.gov/>) and Google Scholar (<https://scholar.google.com/>). The ADMET descriptors in absorption are Caco-2₂ permeability, Intestinal absorption (human), water-solubility, p-glycoprotein substrate, p-glycoprotein 1 and 2 inhibitors, skin permeability; in Distribution are Volume of distribution (VDss) Human, Blood brain barrier (BBB) permeability, Fraction unbound (Human), CNS permeability; in Metabolism are Cytochrome P450 inhibitors, CYP2D6/CYP3A4 substrate; in Excretion are Renal OCT2 substrate, Total Clearance; in Toxicity are Rat LD50, *T. Pyriformis* toxicity, AMES Toxicity, Minnow Toxicity, Maximum Tolerated Dose, Hepatotoxicity, Oral Rat Chronic Toxicity, Skin Sensitization, hERG 1 and 2 inhibitors etc. We enumerated all the above stipulations for all these 154 compounds using the ADMET tool and choose the best out of these, which are employed for molecular docking analysis.

2.5 Molecular docking simulation

By employing ADMET prediction, 18 compounds were picked and further re-docking was employed to them through the software AutoDock Vina (Trott and Olson 2010) with the control ligand DK1. Prior to the docking the preparation of the protein and ligands were performed using the AutDock Tools (Morris et al. 2009). The protein was prepared by adding all the hydrogens, Kollman charges and by assigning the AD4 type radii. After that the protein is saved in to the *.pdbqt* file format. In the ligand preparation, all the hydrogens and Gasteiger charges were added. After this the ligands were saved as *.pdbqt* file. The setting of the grid box was: Center_X = 3.909, Center_Y = 38.484, Center_Z = -18.612, numbers of points were set as, X_dimension = 40, Y_dimension = 40, Z_dimension = 40 with 0.419 Å spacing. After this step the docking were carried out to get the binding affinity and binding pose using Autodock Vina. For each ligand, 8 binding poses were produced and the analysis is done on the basis of least binding energy and the best binding pose. AutoDock Vina is more efficient

when compared to AutoDock because of its rapid docking of ligands and more accurate results (Trott and Olson 2010).

2.6 Density functional theory calculations

The Density functional theory (DFT) analysis has been carried out to decipher the electron transport potential and electronic properties of the selected lead compounds (Matysiak 2007; Zhenming et al. 2011). The geometry of all the ligands was optimized and then they are employed for the DFT calculation through Argus lab software (V: 4.0.1). The HOMO (highest occupied molecular orbital) and LUMO (lowest unoccupied molecular orbital) are commonly known as frontier molecular orbitals and were found to give extremely applicable information about electron density clouds around the molecule (Genc et al. 2015). The HOMO and LUMO are considered as a nonbonding type and π molecular orbital, respectively. The HOMO and LUMO are favorable for the electrophilic and nucleophilic attacks, respectively. E_{HOMO} and E_{LUMO} are the quantum chemical parameter in which E_{HOMO} has the capability of donating the electron while E_{LUMO} can accept the electron from the partner interactor. The higher value of E_{HOMO} signifies that the compound can easily donate the electron without much energy requirement and vacate the molecular orbital (Gece and Bilgiç 2009). The ΔE (energy gap) represents the difference between the HOMO and LUMO energy levels and is calculated by the $\Delta E = E_{\text{LUMO}} - E_{\text{HOMO}}$ (Lu et al. 2010). It is a key parameter that defines the reactivity of the lead compounds towards the NMDAR binding site. Less energy gap represents the reactivity of the lead compounds which leads to an increase in the electron-donating efficiency and represents that it donate its electron from the last occupied orbital with very less energy (Tripathy et al. 2019).

2.7 Molecular dynamics simulation

The Molecular dynamics simulation (MDS) is a very powerful technique to reveal the structural conformation of proteins (Pathak et al. 2022a, b). GROMACS 2018.2 suite (Abraham et al. 2015) was used to perform molecular dynamics (MD) simulations on the apo-NMDAR, NMDAR-DK1, NMDAR-ZINC4258884, NMDAR-ZINC8635472 and NMDAR-ZINC15675934 complexes. A rhombic dodecahedral box having a distance of 10 Å from the closest edge was used to solvate the complexes, thereby, adding more than 19,734 water molecules. Also, for the purpose of neutralizing the system, 4 Cl⁻ counter ions were included. For the ligand GAFF force field was used; for protein, Amber ff99SB-ILDN force field was used and TIP3P model was used for water. Using an isobaric-isothermal ensemble, production runs were performed for 1 ns, after undergoing a standard preparation routine including energy minimization,

annealing, and equilibration. Long range electrostatic interactions were calculated by Particle Mesh Ewald method (Darden et al. 1993). For the computation of Lennard-Jones and Coulomb interactions, 1.0 nm radius cut-off was used. The LINCS algorithm (Hess et al. 1997) was used to constrain the H-bond lengths. The time step was maintained at 2 fs for the simulation. For predicting the short-range non-bonded interaction, 10 Å cut-off distance was used. 1.6 Å Fourier grid spacing was used for the PME method for long-range electrostatics. All bonds including H-bond were fixed by Shake algorithm (Ryckaert et al. 1977). The systems were stabilized after energy minimization. Then position restraint simulation of 1 ns was carried out under NVT and NPT conditions (Bera et al. 2018; Bera 2021). Finally, 100 ns MDS were performed for the final analysis (Bera et al. 2021, p. 19; Ajjarapu et al. 2021). Undergoing subsequent analysis, after the elimination of the protein rotation by least-squares fit with respect to the C α atoms. Various other analyses have also been carried out to predict the protein-ligand stability (Rajendran et al. 2020). The free energy landscape was predicted using the *gmx sham* tool of Gromacs (Rajendran et al. 2018).

3 Results

3.1 Virtual screening analysis

The virtual screening has been carried out using Smina-A fork of AutoDock Vina and idock software. We have screened 98,072 compounds against the NMDAR and binding affinity of all these compounds were displayed in Supplementary Table S1. The ZINC04277685 was the highest binding energy compound in Smina virtual screening result with -13.1 kcal/mol binding affinity while idock showed ZINC04258868 as the top compound having the binding affinity value as -13.29 kcal/mol. The difference between these top compounds prediction could be the result of different tools while we have taken the consensus result from both the software. The ZINC39410302 is predicted as the lowest binding affinity compound by Smina virtual screening with -3.9 kcal/mol binding affinity while idock predicted ZINC01690436 as the lowest binding affinity compound with -3.99 kcal/mol. After that, we have taken 154 compounds which are showing ≥ -11.5 kcal/mol binding affinity in both the tools and used for the ADMET prediction.

3.2 ADMET descriptors analysis

ADMET stands for Absorption, Distribution, Metabolism, Excretion, and Toxicity. These features are essential in support of drug designing studies and the drug cannot be enter into the market until it fulfills the ADMET requirements.

Therefore, this step is of utmost important. We employed the selected 154 compounds in the ADMET analysis via the pkCSM server. As we are targeting the Central Nervous System, the BBB is the most important parameter here, 31 compounds were rejected based on BBB. The second priority was given to CNS permeability and 12 compounds were rejected according to this. The next priority was given to the absorption of the drug, as it is an important factor for oral drug discovery. In the absorption category, HIA is evaluated, as it tells us if the drug is absorbed in the intestine or not, based on this, no compound was rejected. Caco-2 cell permeability is also checked to see the drug assimilation in the large intestine, 94 compounds were rejected based on this. Next, in absorption, it is checked that whether a given compound is likely to be a substrate of p-glycoprotein (Pgp) or not. Pgp usually functions as a biological barrier by excluding xenobiotics and toxins out from the cells, 2 compounds were rejected in this step (Supplementary Tables S2 and S3).

Next, we check for the Cytochrome P450 barriers (CYP450). Here it is assessed that for a given isoform, the potential drug molecule is likely to be a CYP450 inhibitor or not. This enzyme is present in the liver and is responsible for the detoxification of the xenobiotics. Hence, it can deactivate many drugs. Here we look for the CYP2D6/CYP3A4 substrate, which lets us know that whether the drug can be metabolized so that it can be removed from the body. In the case of CYP2D6, we got only 11 positive results whereas in the case of CYP3A4 we got 151 positive results and only 3 compounds were rejected (Supplementary Table S4).

Another important criterion for drug discovery is to assess the toxicity of the potential drug molecules. Even if the efficacy of the drug is high, it cannot be launched in the market if it is toxic, we checked for the AMES toxicity which tells us about the possibility of carcinogenicity, based on this, 66 compounds were rejected. hERG is an ion channel known for the electrical activity of the heart. hERG codes for the potassium channels. Inhibition of these channels leads to long QT-syndrome which leads to the fatal ventricular arrhythmia. Therefore, we have to look for the drug candidates that do not inhibit hERG channels, keeping this as the basis, further 2 compounds were rejected (Supplementary Table S5). Considering all these parameters, a total of 18 potential drug targets were selected from the 154 compounds.

3.3 Molecular docking simulation analysis

The 18 compounds chosen via ADMET analysis along with the control compound DK1 were submitted to molecular docking through AutoDock Vina software. The control compound is redocked using the AutoDock Vina, giving the binding affinity to be as $-8.6 \text{ kcal.mol}^{-1}$. The compound ZINC705167 illustrated the highest binding affinity

of $-12.7 \text{ kcal.mol}^{-1}$ and the compound ZINC705168 illustrated the lowest binding energy of $-8.7 \text{ kcal.mol}^{-1}$, followed by the least binding affinity of the control compound of $-8.6 \text{ kcal.mol}^{-1}$. The binding energy, hydrogen bonds, interacting residues from AutoDock Vina, Smina and idock are tabulated in the Supplementary Table S6 for all the chosen selected ligands along with the DK1. The respective ZINC IDs, binding affinities, 2D chemical structure for the top 3 selected compounds with DK1 are shown in Table 1.

3.4 Selected compounds analysis

3.4.1 DK1

The DK1 exhibited the binding affinity of -8.6 , -8.6 and $-8.71 \text{ kcal.mol}^{-1}$ using Autodock Vina, Smina, and idock, respectively. The DK1 showed less binding affinity in comparison to all the other ligands which represents that predicted hits are good as compare to DK1. We have seen 2, 4 and 5 hydrogen bonds from Autodock Vina, Smina, and idock, respectively. We have seen many common residues such as Pro124 and Thr126 etc. from all three software's. The residue interaction diagram is shown in Fig. 3A. The detailed residues are shown in the Supplementary Table S6.

3.4.2 ZINC4258884

The ZINC4258884 exhibited the binding affinity of -12.5 , -12.5 , and $-12.77 \text{ kcal.mol}^{-1}$ using Autodock Vina, Smina, and idock, respectively. We have analyzed the Autodock Vina docking complex which is showing one hydrogen bond with the Ser180 and various other residues are involved in the hydrophobic interaction. Various common residues are also found in all three docking softwares. The residue interaction diagram is shown in Fig. 3B. The detailed residues are shown in the Supplementary Table S6.

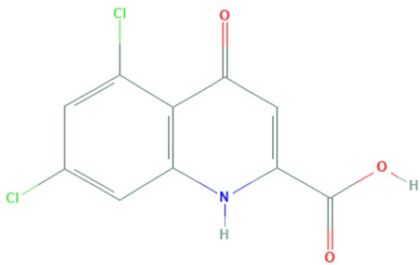
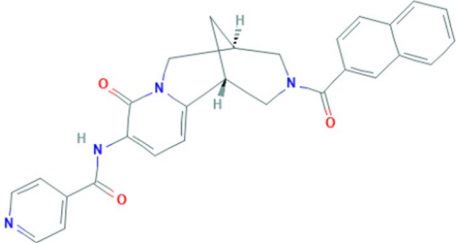
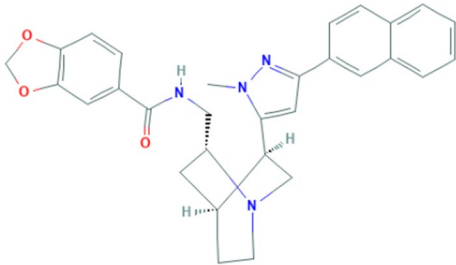
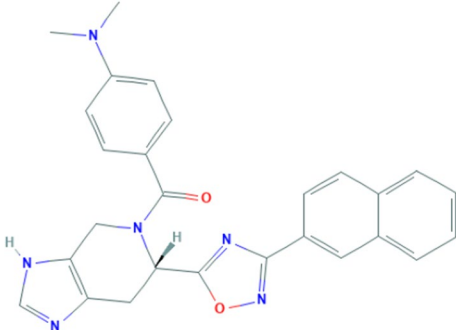
3.4.3 ZINC8635472

The ZINC8635472 exhibited the binding affinity of -12.1 , -12.1 , and $-12.18 \text{ kcal.mol}^{-1}$ using Autodock Vina, Smina, and idock. Using AutoVina software, the complex forms 1 hydrogen bond with Thr126. The complex is also stabilized by many hydrophobic interactions. Common residues are also found in all three docking softwares. The residue interaction diagram is shown in Fig. 3C. The detailed residues are shown in the Supplementary Table S6.

3.4.4 ZINC15675934

The ZINC15675934 is also docked by all the software against the NMDAR. It showed -11.9 , -12.2 , and $-12.3 \text{ kcal.mol}^{-1}$ from Autodock Vina, Smina, and idock

Table 1 Details of the three selected compounds with control compound DK1

ZINC ID	Structure	Autodock Vina (kcal.mol ⁻¹)	Smina (kcal.mol ⁻¹)	idock (kcal.mol ⁻¹)
DK1		- 8.6	- 8.6	- 8.71
ZINC4258884		- 12.5	- 12.5	- 12.77
ZINC8635472		- 12.1	- 12.1	- 12.18
ZINC15675934		- 11.9	- 12.2	- 12.3

ZINC ID, 2D structures and binding affinity obtained after molecular docking are shown

software, respectively. We have not seen any hydrogen bonds between the NMDAR and ZINC15675934 through the Autodock Vina while the complex is seen to be stabilized by many other interactions like hydrophobic interactions etc. The residue interaction diagram is shown in Fig. 3D. The detailed residue interaction is shown in the Supplementary Table S6.

3.5 Density functional theory analysis

The electronic properties of the selected three hits were analyzed using the DFT analysis. The chemical stability of the selected hits was studied by calculating the energy gap between the E_{HOMO} and E_{LUMO} (Johnson et al. 2010). Since the HOMO and LUMO orbitals play a key important role

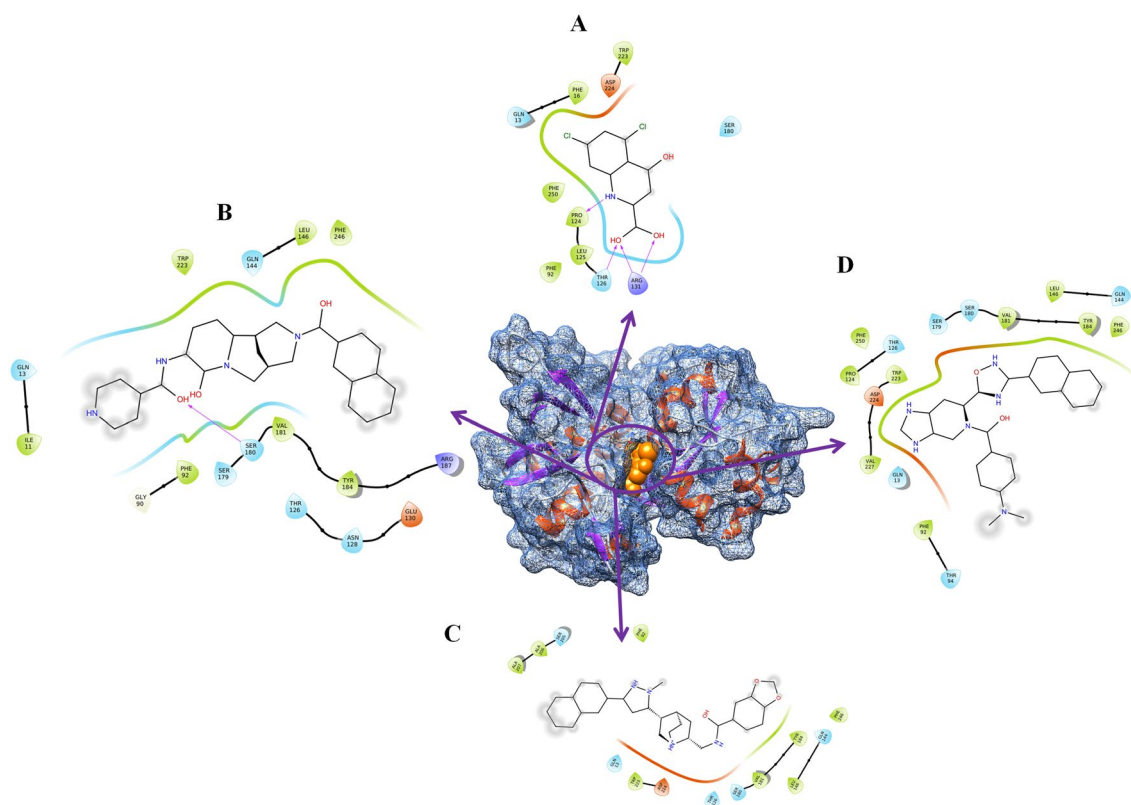


Fig. 3 The ligand interaction diagram. **A** DYRK1A-DK1. **B** DYRK1A-ZINC4258884. **C** DYRK1A-ZINC8635472 and **D** DYRK1A-ZINC15675934

Table 2 Orbital energy values of lead compounds with their energy band

Name	HOMO energy (kcal/mol)	LUMO energy (kcal/mol)	LUMO–HOMO (ΔE)
ZINC4258884	– 11.28	– 8.71	– 2.57
ZINC8635472	– 11.24	– 8.64	– 2.6
ZINC15675934	– 10.87	– 10.57	– 0.3

in charge transfer between the orbitals during a chemical reaction. The E_{HOMO} and E_{LUMO} values and their energy gap are calculated for the selected three lead compounds and shown in Table 2. The energy gap is ranging between 0.30 to 2.57 eV for the selected hits.

We have seen the highest energy gap of – 2.60 eV for ZINC8635472 which indicates that this compound cannot quickly donate its electron. It requires more amount of energy to donate the electron towards the LUMO orbital of the binding site amino acid. The ZINC15675934 showed the lowest energy gap 0.30 eV which represents that it is a highly reactive and unstable compound. It can easily donate the electron and participates in the bonding. The value of the E_{gap} decreases according to the

following order: ZINC8635472 (2.60 eV) > ZINC4258884 (2.57 eV) > ZINC15675934 (0.30 eV). Hence, the reactivity order also increases according to: ZINC8635472 (2.60 eV) > ZINC4258884 (2.57 eV) > ZINC15675934 (0.30 eV) where the most reactive is clearly ZINC15675934 (0.30 eV). The order of reactivity increases conforms to the decreases in energy gap values. The HOMO and LUMO distribution of three identified hit compounds (ZINC4258884, ZINC8635472 and ZINC15675934) is depicted in Fig. 4. The blue and red color represents the HOMO and LUMO distribution which represents the possible active sites present in the hit molecules (Fig. 4).

3.6 Molecular dynamics simulation

The Molecular dynamics simulation is a widely used technique to evaluate the docked stability of protein-ligand complex. Therefore, this study comprises of using MDS for the validation of docking complexes. We have selected 3 top complexes with the apo-NMDAR and NMDAR-DK1 for the 100 ns simulation. Various structural parameters such as root mean square deviation (RMSD), root mean square fluctuation (RMSF), Radius of gyration (Rg), Solvent accessible surface area (SASA), number of hydrogen bonds and

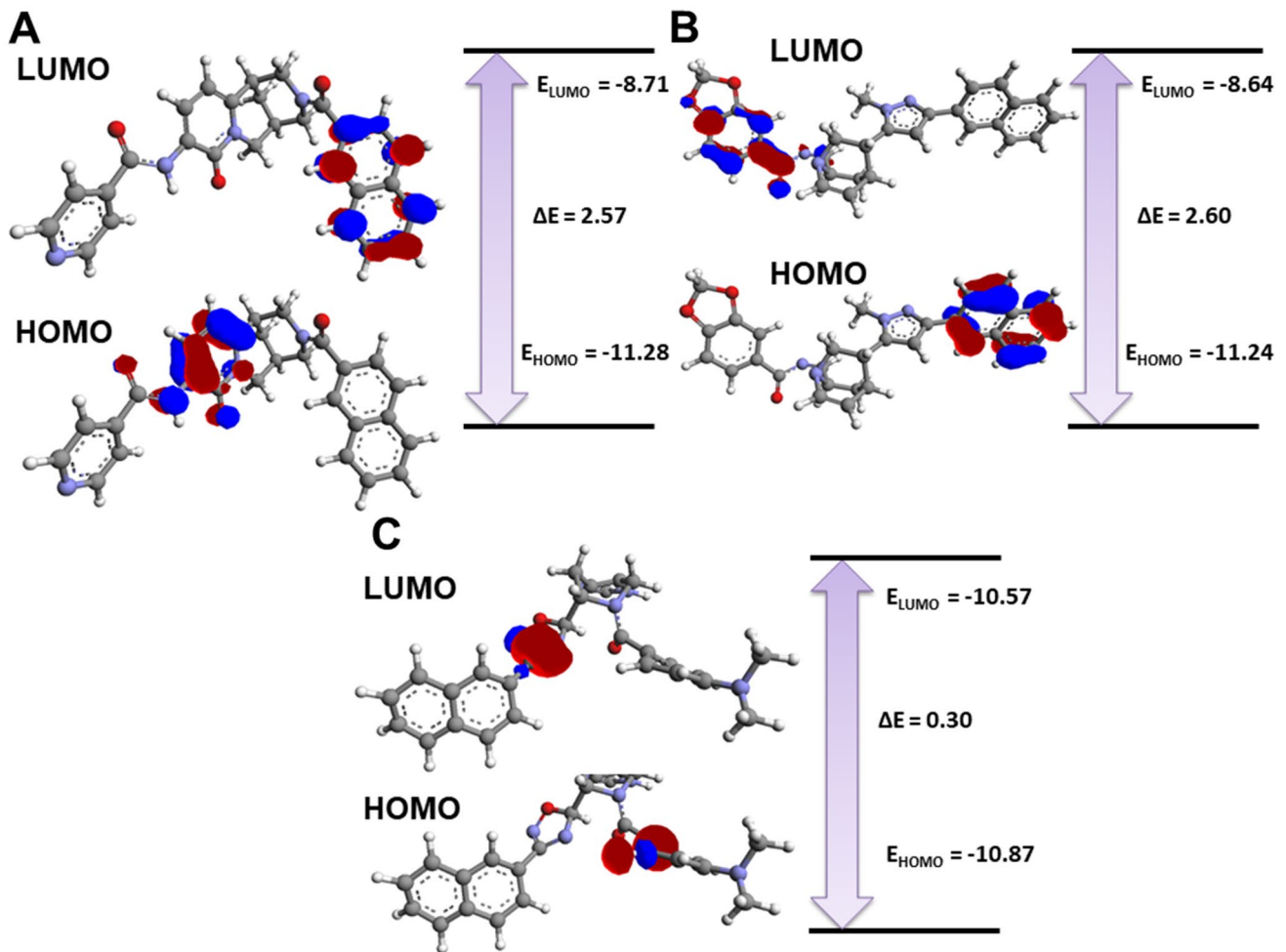


Fig. 4 Charge distribution of HOMO and LUMO with their energy band. **A** ZINC4258884 **B** ZINC8635472 and **C** ZINC15675934

Table 3 Average MDS value for all the complexes

Complex	RMSD (nm)	RMSF (nm)	Rg (nm)	SASA (nm ²)	H-bonds
apo-NMDAR	0.54	0.17	2.16	155.81	–
NMDAR-DK1	0.53	0.13	2.16	155.25	4–6
NMDAR-ZINC4258884	0.27	0.10	2.06	153.45	0–2
NMDAR-ZINC8635472	0.48	0.18	2.19	157.31	1–4
NMDAR-ZINC15675934	0.45	0.12	2.18	154.85	0–2

Principal component analysis (PCA) were carried out. The average value for all the systems were shown in Table 3.

3.6.1 Stability analysis

For the purpose of prediction of the stability of simulation, the RMSD has been carried out. We have computed the RMSD value for 100 ns and plotted it in Fig. 5A. It represents the deviation from the initial structure to the next structure. The Fig. 5A represents that after the 50 ns all the simulations got the stability and can be used for the

analysis. The average RMSD for apo-NMDAR, NMDAR-DK1, NMDAR-ZINC4258884, NMDAR-ZINC8635472 and NMDAR-ZINC15675934 was 0.54, 0.53, 0.27, 0.48 and 0.45 nm, respectively (Table 3). The average RMSD after ligand binding for all the complexes got the stability as compare to apo-NMDAR and control ligand DK1. The predicted hits also showed less RMSD value in comparison to the DK1 and representing a well-stable complex. Hence from here, we have predicted that all our complexes got the equilibrations and the simulation trajectories are

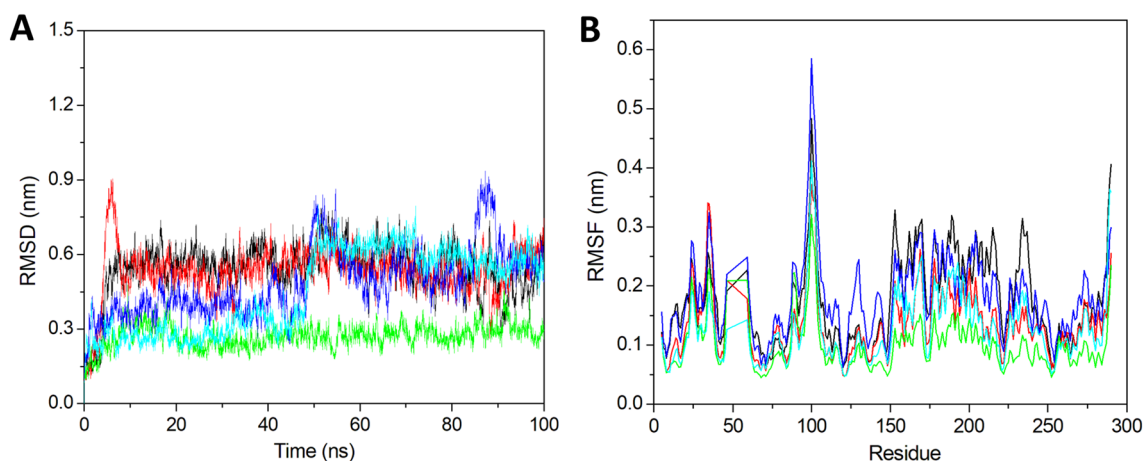


Fig. 5 RMSD and RMSF. **A** RMSD of 100 ns at 300 K. **B** RMSF for all the residues. The black, red, green, blue, and cyan represents apo-NMDAR, NMDAR-DK1, NMDAR-ZINC4258884, NMDAR-ZINC8635472, and NMDAR-ZINC15675934, respectively

producing accurate results. Hence, we considered last 50 ns trajectories for further analysis.

3.6.2 Residue mobility analysis

The residue level mobility analysis using the RMSF analysis was carried out. This is a very important analysis in the case of NMDAR because it is an ion channel and very flexible in nature. Hence it will show the higher fluctuation in several residues. We have plotted the residue mobility in the Fig. 5B. In the Fig. 5B, we have seen very high fluctuation between the residues 94–106. The plot showed higher fluctuation in the maximum region of the protein as compared to the general fluctuation due to the ion channel nature of the NMDAR. The average RMSF for apo-NMDAR, NMDAR-DK1, NMDAR-ZINC4258884, NMDAR-ZINC8635472 and NMDAR-ZINC15675934 was 0.17, 0.13, 0.10, 0.18 and 0.12 nm, respectively (Table 3). The highest fluctuation is showed by NMDAR-ZINC8635472 whilst in comparison to the apo-NMDAR and NMDAR-DK1, NMDAR-ZINC4258884 and NMDAR-ZINC15675934 were seen to show a lesser fluctuation. It displayed the stability of NMDAR-ZINC4258884 and NMDAR-ZINC15675934 and showed their potential use as a lead compound against NMDAR.

3.6.3 Compactness analysis

The compactness of the complexes has been analyzed using the Rg analysis. The Rg has been measured from the radius of the protein and represents the compactness of the protein. Hence here also we have calculated the Rg for the last 50 ns stabilized trajectory. It is plotted in Fig. 6A. In Fig. 6A we can see that NMDAR-ZINC4258884 showed

very least value as compare to all other complexes. Other complexes and apo-NMDAR showed a similar type of Rg value. The average Rg value for apo-NMDAR, NMDAR-DK1, NMDAR-ZINC4258884, NMDAR-ZINC8635472, and NMDAR-ZINC15675934 was 2.16, 2.16, 2.06, 2.19, and 2.18 nm, respectively (Table 3). Here also the NMDAR-ZINC8635472 showed the highest value as compare to all others while NMDAR-ZINC4258884 and NMDAR-ZINC15675934 showed the good Rg value and showing less fluctuation. Hence from here also we can say that NMDAR-ZINC4258884 and NMDAR-ZINC15675934 are stable complexes in the respect of Rg analysis.

3.6.4 Solvent accessible surface area analysis

The SASA has been carried out for the prediction of the ligand-induced solvent-accessible area changes. We worked upon using the last 50 ns trajectory and calculated the SASA value and plotted it in Fig. 6B. The Fig. 6B showed a similar type of pattern for all the systems. Hence, we have analyzed the average SASA value for all the systems. The average SASA value for apo-NMDAR, NMDAR-DK1, NMDAR-ZINC4258884, NMDAR-ZINC8635472, and NMDAR-ZINC15675934 was 155.81, 155.25, 153.45, 157.31, and 154.85 nm² (Table 3). Here also we have found that NMDAR-ZINC8635472 is showing the highest SASA value in comparison to the other two complexes. Comparing the results with control compound DK1 and apo-NMDAR, the values for NMDAR-ZINC4258884 and NMDAR-ZINC15675934 were seen to be less. The SASA result also agrees with RMSD, RMSF, and Rg results that NMDAR-ZINC4258884 and NMDAR-ZINC15675934 are the stable complexes.

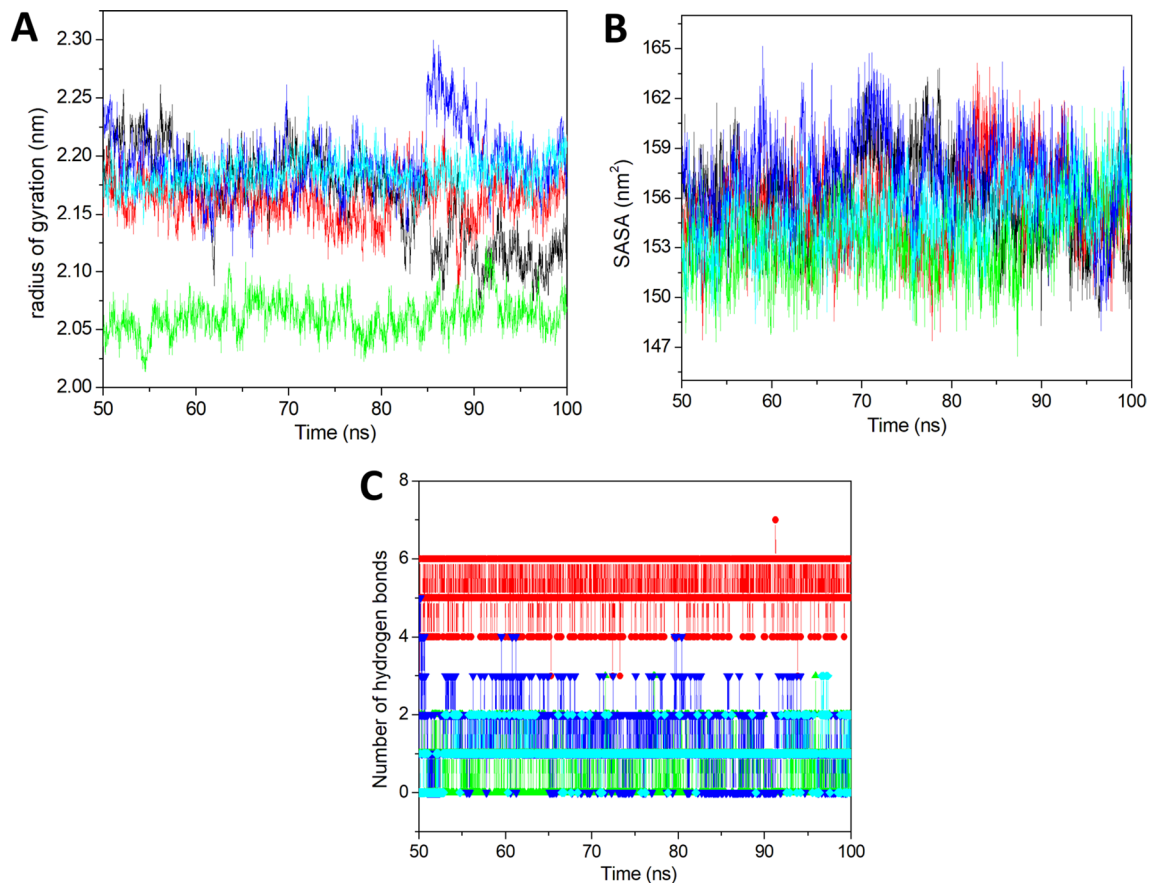


Fig. 6 Radius of gyration, SASA and Number of hydrogen bonds. **A** Radius of gyration vs. time for all the systems. **B** SASA value vs. time for all the systems. **C** Number of hydrogen bonds vs. time. All the values were computed via the last 50 ns trajectory. The black,

red, green, blue, and cyan represents apo-NMDAR, NMDAR-DK1, NMDAR-ZINC4258884, NMDAR-ZINC8635472, and NMDAR-ZINC15675934, respectively

3.6.5 Hydrogen bonds analysis

After that, the number of hydrogen bonds for the last 50 ns was computed and was plotted in Fig. 6C. The hydrogen bonds are crucial for ligand-protein stability. From the Fig. 6C, we can see that NMDAR-DK1 exhibited highest number of hydrogen bonds in comparison to all the estimated complexes. The NMDAR-DK1 showed the average 4-6 hydrogen bonds throughout the simulation. After that NMDAR-ZINC8635472 showed more hydrogens bonds such as 1-4 for all simulations. The NMDAR-ZINC4258884 and NMDAR-ZINC15675934 showed 0-2 hydrogen bonds throughout the simulation (Table 3). The hydrogen bond analysis represents the stability of all the complexes and a greater number of hydrogen bonds is observed in the DK1.

3.6.6 Principal component analysis

The PCA analysis has been carried out for predicting the correlated motions after ligand binding. Here, the

calculation of the eigenvalue vs. and eigenvector was performed. Due to the clear depiction of the result only the first 40 eigenvectors were selected for the analysis and were plotted in Fig. 7A.

In the Fig. 7A we can see that NMDAR-ZINC8635472 is showing very high motions in comparison to all the other complexes. After this complex, apo-NMDAR showed the higher motions. The NMDAR-ZINC4258884 is showing very few motions and stable complex as compare to all other systems. To clearly understand the motions induced by ligand binding, we have computed the correlated motions (percentage wise) for the first 10 eigenvectors. The apo-NMDAR, NMDAR-DK1, NMDAR-ZINC4258884, NMDAR-ZINC8635472, and NMDAR-ZINC15675934 showed 90.62%, 86.49%, 74.34%, 91.03%, and 84.15% correlated motions. Here also we can see that NMDAR-ZINC8635472 and apo-NMDAR are showing very high motions while NMDAR-ZINC4258884 and NMDAR-ZINC15675934 are showing the lowest motions and represents the stable complex.

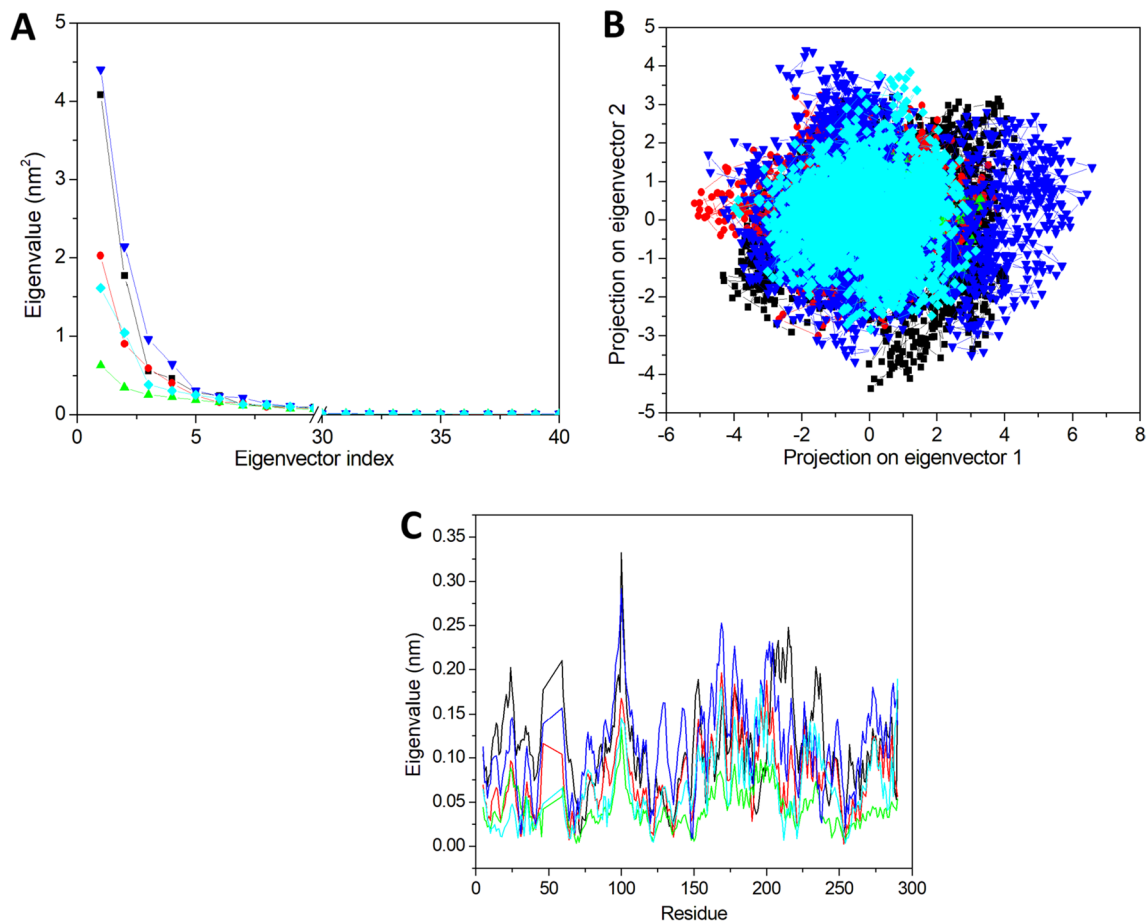


Fig. 7 Principal Component analysis. **(A)** Eigenvalue vs. first 40 eigenvector at 300 K. **(B)** 2D projection plot for all the selected complexes. **(C)** EigRMSF vs. residue for all the systems. All the values were computed from the last 50 ns trajectory. The black,

red, green, blue, and cyan represents apo-NMDAR, NMDAR-DK1, NMDAR-ZINC4258884, NMDAR-ZINC8635472, and NMDAR-ZINC15675934, respectively

From here, we have seen that the overall dynamics of the protein is accountable for the first few eigenvectors. Hence, the first two eigenvectors were selected and plotted against each other in phase space and shown in Fig. 7B. The Fig. 7B represents that NMDAR-ZINC15675934 and NMDAR-ZINC4258884 is the most stable cluster in comparison to all other complexes. These complexes showed very stable cluster which represents the complex stability. After these two the NMDAR-DK1 is showing the stable cluster. We have seen a very wide and dispersed cluster for the NMDAR-ZINC8635472 and apo-NMDAR. The 2D projection report also represents that ZINC15675934 and NMDAR-ZINC4258884 are the stable complex as compare to the NMDAR-ZINC8635472.

Lastly, we have predicted the residue-wise correlated motions from the last 50 ns trajectory using only one eigenvector and plotted in Fig. 7C. Here we have seen a similar pattern as like RMSF analysis. We have seen a high peak from residues 87-109. The overall eigRMSF is also

high for all the residues. The apo-NMDAR, NMDAR-DK1, NMDAR-ZINC4258884, NMDAR-ZINC8635472 and NMDAR-ZINC15675934 showing average eigRMSF is 0.11, 0.07, 0.04, 0.11 and 0.06 nm, respectively. Here it was observed that average eigRMSF for apo-NMDAR and NMDAR-ZINC8635472 is high as compare to other complexes. The NMDAR-DK1 is also showing less eigRMSF value while our predicted hits NMDAR-ZINC4258884 and NMDAR-ZINC15675934 are showing very less eigRMSF value and representing the well-stable complexes.

3.6.7 Gibbs free energy landscape analysis

We have taken the first two principal components for the Gibbs free energy landscape calculation. The FEL for all the systems was calculated and shown in Fig. 8. The deep blue color in the plot represents the lowest energy conformation while the red color represents the highest energy conformation. The lower energy transition states

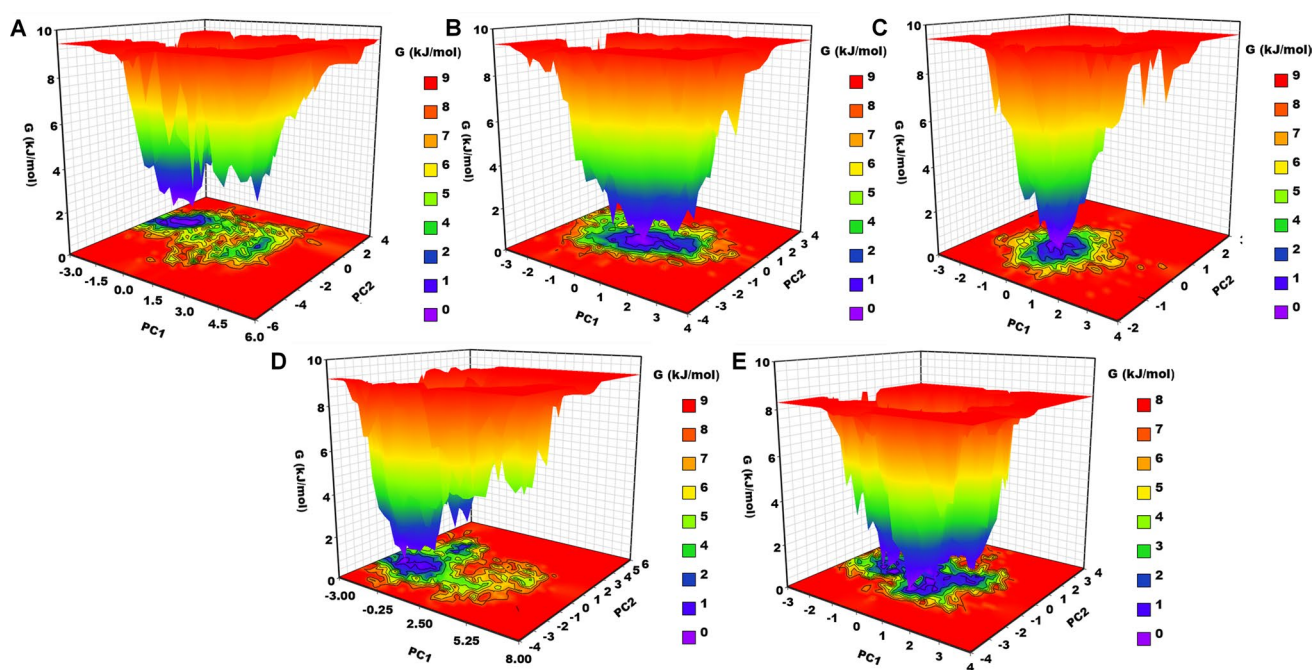


Fig. 8 Gibbs free energy landscape. (A) apo-NMDAR, (B) NMDAR-DK1, (C) NMDAR-ZINC4258884, (D) NMDAR-ZINC8635472 and (E) NMDAR-ZINC15675934

are represented by the deep valley with the blue color. In the case of apo-NMDAR, we have seen blue color enriched energy minima with wide space. It represents the stable cluster. We have also seen a transition state with less blue color and that is separated by a high energy barrier. For the NMDAR-control ligand, we have seen many small wells, but that are not separated by any high energy barrier. Those are nearby each other. It represents that the NMDAR-control ligand has several thermodynamically favorable transitions. The NMDAR-ZINC4258884 showed clear energy minima with one deep well. It represents that this complex is more energetically stable than the control complex and not changing its conformational states very frequently. The NMDAR-ZINC8635472 showed two deep wells but those contain several small energy minima. Those two wells are separated by an energy barrier. It represents that this complex exists in two conformational states. Lastly, we have analyzed the NMDAR-ZINC15675934 complex which showed three energy funnels and all are connected through each other. It is covering the more blue area as compare to other predicted hits as well as the control compound which represents the stable cluster. It symbolizes that NMDAR-ZINC15675934 can get many conformational states and all are thermodynamically favorable. From the overall FEL analysis, we have predicted that the NMDAR-ZINC4258884 and NMDAR-ZINC15675934 are the stable complex and these compounds can act as a lead compound.

The overall PCA and Gibbs FEL result also agrees with the above analysis namely RMSD, RMSF, hydrogen bond analysis and SASA. These all result indicates that out of three complexes the NMDAR-ZINC4258884 and NMDAR-ZINC15675934 are stable and has a potential to act as lead compounds.

4 Conclusion

AD is a progressive neurological disorder mainly affecting old age people. There is no medication available to cure AD. The NMDAR is a key target in the case of AD hence we have targeted the NMDAR with the natural compounds. We started our study with 98,072 compounds and finished with the potential lead compounds using ADMET and cross-docking analysis approach. Finally, three compounds were chosen and MDS study of 100 ns with the apo-NMDAR and NMDAR-DK1 was performed on them. Then we have carried out various structural parameter analyses, in particular RMSF, Rg, SASA, hydrogen bonds analysis, and PCA. From all these analyses, we have proposed that ZINC4258884 and ZINC15675934 can act as a lead compound against the NMDAR to treat AD. The compounds were shortlisted from a pool of compounds using rigorous computational approach. These compounds can be used for the structure activity relation and a common moiety can be found for the QSAR and pharmacophore modeling. The worldwide

scientists can test these compounds employing both *in-vivo* and *in-vitro* methods. These compounds can be used as a lead compound against NMDAR to tackle the various diseases where NMDAR is involved.

Supplementary Information The online version contains supplementary material available at <https://doi.org/10.1007/s13721-022-00374-2>.

Acknowledgements RS and TRS want to thank the ICMR (ISRM/11(53)/2019) for providing the Senior Research Fellowship to RS.

Author contributions TRS conceived the study. GS and RS carried out all the experiments and the data analysis. GS, RS and TRS participated in its overall design and coordination of the study. The first draft of the manuscript was prepared by GS and RS. All authors read and approved the final manuscript.

Declarations

Conflict of interest The authors declare that there are no competing interests.

References

- Abbott JJ, Howlett DR, Francis PT, Williams RJ (2008) Abeta(1–42) modulation of Akt phosphorylation via alpha7 nAChR and NMDA receptors. *Neurobiol Aging* 29:992–1001. <https://doi.org/10.1016/j.neurobiolaging.2007.01.003>
- Abraham MJ, Murtola T, Schulz R et al (2015) GROMACS: high performance molecular simulations through multi-level parallelism from laptops to supercomputers. *SoftwareX* 1–2:19–25. <https://doi.org/10.1016/j.softx.2015.06.001>
- Ajjarapu SM, Tiwari A, Taj G et al (2021) Simulation studies, 3D QSAR and molecular docking on a point mutation of protein kinase B with flavonoids targeting ovarian Cancer. *BMC Pharmacol Toxicol* 22:1–23. <https://doi.org/10.1186/s40360-021-00512-y>
- Armstrong N, Gouaux E (2000) Mechanisms for activation and antagonism of an AMPA-sensitive glutamate receptor: crystal structures of the GluR2 ligand binding core. *Neuron* 28:165–181. [https://doi.org/10.1016/s0896-6273\(00\)00094-5](https://doi.org/10.1016/s0896-6273(00)00094-5)
- Bera K (2021) Binding and inhibitory effect of ravidasvir on 3CLpro of SARS-CoV-2: a molecular docking, molecular dynamics and MM/PBSA approach. *J Biomol Struct Dyn* 0:1–8. <https://doi.org/10.1080/07391102.2021.1896388>
- Bera K, Rani P, Kishor G et al (2018) Structural elucidation of transmembrane domain zero (TMD0) of EcdL: a multidrug resistance-associated protein (MRP) family of ATP-binding cassette transporter protein revealed by atomistic simulation. *J Biomol Struct Dyn* 36:2938–2950. <https://doi.org/10.1080/07391102.2017.1372311>
- Bera K, Reeda VSJ, Babila PR et al (2021) An in silico molecular dynamics simulation study on the inhibitors of SARS-CoV-2 proteases (3CLpro and PLpro) to combat COVID-19. *Mol Simul* 47:1168–1184. <https://doi.org/10.1080/08927022.2021.1957884>
- Blanke ML, Van Dongen AMJ (2009) Activation mechanisms of the NMDA receptor. In: Van Dongen AM (ed) *Biology of the NMDA receptor*. CRC Press/Taylor & Francis, Boca Raton
- Cao J, Hou J, Ping J, Cai D (2018) Advances in developing novel therapeutic strategies for Alzheimer's disease. *Mol Neurodegener* 13:64. <https://doi.org/10.1186/s13024-018-0299-8>
- Companys-Aleman J, Turcu AL, Bellver-Sanchis A et al (2020) A novel NMDA receptor antagonist protects against cognitive decline presented by senescent mice. *Pharmaceutics* 12:E284. <https://doi.org/10.3390/pharmaceutics12030284>
- Danysz W, Parsons CG (2012) Alzheimer's disease, β -amyloid, glutamate, NMDA receptors and memantine—searching for the connections. *Br J Pharmacol* 167:324–352. <https://doi.org/10.1111/j.1476-5381.2012.02057.x>
- Darden T, York D, Pedersen L (1993) Particle mesh Ewald: an N \cdot log(N) method for Ewald sums in large systems. *J Chem Phys* 98:10089–10092. <https://doi.org/10.1063/1.464397>
- Folch J, Petrov D, Etcheto M et al (2016) Current research therapeutic strategies for Alzheimer's disease treatment. *Neural Plast* 2016:8501693. <https://doi.org/10.1155/2016/8501693>
- Gece G, Bilgiç S (2009) Quantum chemical study of some cyclic nitrogen compounds as corrosion inhibitors of steel in NaCl media. *Corros Sci* 51:1876–1878. <https://doi.org/10.1016/j.corsci.2009.04.003>
- Genc ZK, Tekin S, Sandal S et al (2015) Synthesis and DFT studies of structural and some spectral parameters of nickel(II) complex with 2-(2-hydroxybenzoyl)-N-(1-adamantyl) hydrazine carbothioamide. *Res Chem Intermed* 41:4477–4488. <https://doi.org/10.1007/s11164-014-1545-5>
- Hess B, Bekker H, Berendsen HJC, Fraaije JGEM (1997) LINCS: a linear constraint solver for molecular simulations. *J Comput Chem* 18:1463–1472. [https://doi.org/10.1002/\(SICI\)1096-987X\(199709\)18:12%3c1463::AID-JCC4%3e3.0.CO;2-H](https://doi.org/10.1002/(SICI)1096-987X(199709)18:12%3c1463::AID-JCC4%3e3.0.CO;2-H)
- Ikonomidou C, Turski L (2002) Why did NMDA receptor antagonists fail clinical trials for stroke and traumatic brain injury? *Lancet Neurol* 1:383–386. [https://doi.org/10.1016/s1474-4422\(02\)00164-3](https://doi.org/10.1016/s1474-4422(02)00164-3)
- Jewett BE, Thapa B (2021) *Physiology, NMDA receptor*. In: StatPearls. StatPearls Publishing, Treasure Island
- Johnson ER, Yang W, Davidson ER (2010) Spin-state splittings, highest-occupied-molecular-orbital and lowest-unoccupied-molecular-orbital energies, and chemical hardness. *J Chem Phys* 133:164107. <https://doi.org/10.1063/1.3497190>
- Kato T, Duman RS (2020) Rapastinel, a novel glutamatergic agent with ketamine-like antidepressant actions: convergent mechanisms. *Pharmacol Biochem Behav* 188:172827. <https://doi.org/10.1016/j.pbb.2019.172827>
- Kumar A, Nisha CM, Silakari C et al (2016) Current and novel therapeutic molecules and targets in Alzheimer's disease. *J Formos Med Assoc* 115:3–10. <https://doi.org/10.1016/j.jfma.2015.04.001>
- Li H, Leung K, Wong M (2012) idock: a multithreaded virtual screening tool for flexible ligand docking. In: 2012 IEEE Symposium on Computational Intelligence in Bioinformatics and Computational Biology (CIBCB), pp 77–84
- Lindorff-Larsen K, Piana S, Palmo K et al (2010) Improved side-chain torsion potentials for the Amber ff99SB protein force field. *Proteins* 78:1950–1958. <https://doi.org/10.1002/prot.22711>
- Liu J, Chang L, Song Y et al (2019) The role of NMDA receptors in Alzheimer's disease. *Front Neurosci*. <https://doi.org/10.3389/fnins.2019.00043>
- Lu Y, Wang Y, Zhu W (2010) Nonbonding interactions of organic halogens in biological systems: implications for drug discovery and biomolecular design. *Phys Chem Chem Phys* 12:4543–4551. <https://doi.org/10.1039/B926326H>
- Matysiak J (2007) Evaluation of electronic, lipophilic and membrane affinity effects on antiproliferative activity of 5-substituted-2-(2,4-dihydroxyphenyl)-1,3,4-thiadiazoles against various human cancer cells. *Eur J Med Chem* 42:940–947. <https://doi.org/10.1016/j.ejmech.2006.12.033>
- Morel V, Joly D, Villatte C et al (2018) Preventive effect of oral magnesium in postmastectomy pain: protocol for a randomised,

- double-blind, controlled clinical trial. *BMJ Open* 8:e017986. <https://doi.org/10.1136/bmjopen-2017-017986>
- Morris GM, Huey R, Lindstrom W et al (2009) AutoDock4 and AutoDockTools4: automated docking with selective receptor flexibility. *J Comput Chem* 30:2785–2791. <https://doi.org/10.1002/jcc.21256>
- Newcomer JW, Farber NB, Olney JW (2000) NMDA receptor function, memory, and brain aging. *Dialogues Clin Neurosci* 2:219–232
- Pathak RK, Lim B, Park Y, Kim J-M (2022a) Unraveling structural and conformational dynamics of DGAT1 missense nsSNPs in dairy cattle. *Sci Rep* 12:4873. <https://doi.org/10.1038/s41598-022-08833-6>
- Pathak RK, Seo Y-J, Kim J-M (2022b) Structural insights into inhibition of PRRSV Nsp4 revealed by structure-based virtual screening, molecular dynamics, and MM-PBSA studies. *J Biol Eng* 16:4. <https://doi.org/10.1186/s13036-022-00284-x>
- Pettersen EF, Goddard TD, Huang CC et al (2004) UCSF Chimera—a visualization system for exploratory research and analysis. *J Comput Chem* 25:1605–1612. <https://doi.org/10.1002/jcc.20084>
- Pires DEV, Blundell TL, Ascher DB (2015) pkCSM: predicting small-molecule pharmacokinetic and toxicity properties using graph-based signatures. *J Med Chem* 58:4066–4072. <https://doi.org/10.1021/acs.jmedchem.5b00104>
- Rajendran V, Shukla R, Shukla H, Tripathi T (2018) Structure-function studies of the asparaginyl-tRNA synthetase from *Fasciola gigantica*: understanding the role of catalytic and non-catalytic domains. *Biochem J* 475:3377–3391. <https://doi.org/10.1042/BCJ20180700>
- Rajendran V, Kandasamy S, Gupta A, et al (2020) Insilico identification of potential antivirals and molecular dynamics against SARS-CoV2 main protease and RBD of spike protein. <https://doi.org/10.26434/chemrxiv.13181117.v1>
- Ryckaert J-P, Ciccotti G, Berendsen HJC (1977) Numerical integration of the cartesian equations of motion of a system with constraints: molecular dynamics of n-alkanes. *J Comput Phys* 23:327–341. [https://doi.org/10.1016/0021-9991\(77\)90098-5](https://doi.org/10.1016/0021-9991(77)90098-5)
- Shukla R, Singh TR (2020a) Virtual screening, pharmacokinetics, molecular dynamics and binding free energy analysis for small natural molecules against cyclin-dependent kinase 5 for Alzheimer's disease. *J Biomol Struct Dyn* 38:248–262. <https://doi.org/10.1080/07391102.2019.1571947>
- Shukla R, Singh TR (2020b) Identification of small molecules against cyclin dependent kinase-5 using chemoinformatics approach for Alzheimer's disease and other tauopathies. *J Biomol Struct Dyn* 0:1–13. <https://doi.org/10.1080/07391102.2020.1844050>
- Shukla R, Singh TR (2021) High-throughput screening of natural compounds and inhibition of a major therapeutic target HsGSK-3 β for Alzheimer's disease using computational approaches. *J Genet Eng Biotechnol* 19:61. <https://doi.org/10.1186/s43141-021-00163-w>
- Shukla R, Shukla H, Tripathi T (2018) Structural and energetic understanding of novel natural inhibitors of *Mycobacterium tuberculosis* malate synthase. *J Cell Biochem* 120:2469–2482
- Shukla R, Munjal NS, Singh TR (2019) Identification of novel small molecules against GSK3 β for Alzheimer's disease using chemoinformatics approach. *J Mol Graph Model* 91:91–104. <https://doi.org/10.1016/j.jmglm.2019.06.008>
- Shukla R, Shukla H, Tripathi T (2021) Structure-based discovery of phenyl-diketo acids derivatives as *Mycobacterium tuberculosis* malate synthase inhibitors. *J Biomol Struct Dyn* 39:2945–2958. <https://doi.org/10.1080/07391102.2020.1758787>
- Sterling T, Irwin JJ (2015) ZINC 15—ligand discovery for everyone. *J Chem Inf Model* 55:2324–2337. <https://doi.org/10.1021/acs.jcim.5b00559>
- Tabuteau H, Jones A, Anderson A et al (2022) Effect of AXS-05 (dextromethorphan-bupropion) in major depressive disorder: a randomized double-blind controlled trial. *Am J Psychiatry* 179:490–499. <https://doi.org/10.1176/appi.ajp.21080800>
- Takahashi H, Xia P, Cui J et al (2015) Pharmacologically targeted NMDA receptor antagonism by NitroMemantine for cerebrovascular disease. *Sci Rep* 5:14781. <https://doi.org/10.1038/srep14781>
- Tripathy S, Sahu SK, Azam MA, Jupudi S (2019) Computer-aided identification of lead compounds as Staphylococcal epidermidis FtsZ inhibitors using molecular docking, virtual screening, DFT analysis, and molecular dynamic simulation. *J Mol Model* 25:360. <https://doi.org/10.1007/s00894-019-4238-6>
- Trott O, Olson AJ (2010) AutoDock Vina: improving the speed and accuracy of docking with a new scoring function, efficient optimization and multithreading. *J Comput Chem* 31:455–461. <https://doi.org/10.1002/jcc.21334>
- Verma S, Kumar A, Tripathi T, Kumar A (2018) Muscarinic and nicotinic acetylcholine receptor agonists: current scenario in Alzheimer's disease therapy. *J Pharm Pharmacol* 70:985–993. <https://doi.org/10.1111/jphp.12919>
- Wang R, Reddy PH (2017) Role of glutamate and NMDA receptors in Alzheimer's disease. *J Alzheimers Dis JAD* 57:1041–1048. <https://doi.org/10.3233/JAD-160763>
- Weller J, Budson A (2018) Current understanding of Alzheimer's disease diagnosis and treatment. *F1000Research*. <https://doi.org/10.12688/f1000research.14506.1>
- Zhang Y, Li P, Feng J, Wu M (2016) Dysfunction of NMDA receptors in Alzheimer's disease. *Neuro Sci* 37:1039–1047. <https://doi.org/10.1007/s10072-016-2546-5>
- Zhenming D, Heping S, Yufang L et al (2011) Experimental and theoretical study of 10-methoxy-2-phenylbenzo[h]quinoline. *Spectrochim Acta A Mol Biomol Spectrosc* 78:1143–1148. <https://doi.org/10.1016/j.saa.2010.12.067>

Publisher's Note Springer Nature remains neutral with regard to jurisdictional claims in published maps and institutional affiliations.

Springer Nature or its licensor holds exclusive rights to this article under a publishing agreement with the author(s) or other rightsholder(s); author self-archiving of the accepted manuscript version of this article is solely governed by the terms of such publishing agreement and applicable law.